SCIENTIFIC PAPERS
OF THE UNIVERSITY OF PARDUBICE
Series A
Faculty of Chemical Technology
2 (1996)

KINETIC ANALYSIS OF NON-ISOTHERMAL CALORIMETRIC DATA

Jiří MÁLEK
Joint Laboratory of Solid State Chemistry
Academy of Sciences of the Czech Republic and University of Pardubice

Received September 20, 1995

A simple and reliable method of kinetic analysis of non-isothermal calorimetric data has been developed. This method allows to find appropriate model characterizing the kinetics of the process studied as well as to calculate reliable kinetic parameters. The application of this method is demonstrated for three different processes:

(i) Curing reaction of an epoxy resin
(ii) Crystallization kinetics of a chalcogenide glass
(iii) Crystallization kinetics of zirconia gel

The reliability of calculated kinetic parameters is tested by comparing calculated an experimental isothermal kinetic data. It is shown that a very good prediction of isothermal behavior can be obtained. Such modeling can be very useful for preparation of materials with defined properties.

Introduction

The extraction of the kinetic information from non-isothermal data obtained by differential scanning calorimery (DSC) is very attractive because DSC technique is easy to use and applicable to many reactions and processes. Non-isothermal

experiments can also be used to extend the temperature range of measurements beyond that accessible to isothermal experiments. Some crystallization processes occur too rapidly to be measured under isothermal conditions because of transients inherently associated with temperature equilibration.

During the last 10 years we have been engaged in the study of possibilities of non-isothermal kinetics. These studies have gradually led to the formulation of a new method of kinetic analysis using special properties of the $y(\alpha)$ and $z(\alpha)$ functions. A software package called TA-system was developed on the basis of this method of kinetic analysis.

This paper summarizes some of results obtained by solving of kinetic problems on different materials such as epoxy resins, chalcogenide glasses and amorphous zirconia gels. The aim was to demonstrate that even in the case of complicated solid state processes in non-isothermal conditions it is possible to get reliable kinetic parameters. These parameters can be used for predictions of reaction extent under isothermal conditions or for construction of time-temperature-transformation (TTT) diagrams which are very useful for preparation of materials with controlled physical properties.

Theory

Kinetic Equation

Assuming the Arrhenius temperature dependence of the rate constant and the kinetic model function $f(\alpha)$, the following rate equation is usually applied for kinetic analysis of non-isothermal calorimetric data[1]

$$\frac{d\alpha}{dt} = A e^{-x} f(\alpha) \tag{1}$$

where A is the pre-exponential factor, $x = E/RT$ is the reduced activation energy and α is the fractional conversion. It is assumed that the rate of conversion is directly proportional to the heat flow $\phi = dH/dt$, associated with the process under study

$$\frac{d\alpha}{dt} = \frac{\phi}{\Delta H} \tag{2}$$

ΔH being the enthalpy change of the process. Combining equations (1) and (2), the heat flow ϕ measured by DSC technique can be described by the equation

$$\phi = \Delta H A e^{-x} f(\alpha) \tag{3}$$

The kinetic model function $f(\alpha)$ is derived on the basis of physico-geometric assumptions on the movement of reaction interface and the mathematical formulae of the commonly used $f(\alpha)$ functions are summarized in Table I. The aim of the kinetic analysis of DSC data is to find the most appropriate kinetic

model which gives the best description of the studied process and allows the calculation of reliable values for the Arrhenius parameters E and A.

Table I Basic kinetic model functions $f(\alpha)$, together with their integral form $g(\alpha)$

Model	Symbol	$f(\alpha)$	$g(\alpha)$
Phase Boundary Reaction (contracting area)	R_2	$(1-\alpha)^{1/2}$	$2[1-(1-\alpha)^{1/2}]$
Phase boundary reaction (contracting volume)	R_3	$(1-\alpha)^{1/3}$	$3[1-(1-\alpha)^{1/3}]$
Two dimensional diffusion	D_2	$\frac{-1}{\ln(1-\alpha)}$	$(1-\alpha)\ln(1-\alpha)+\alpha$
Three dimensional diffusion (Jander Eq.)	D_3	$\frac{3(1-\alpha)^{2/3}}{2[1-(1-\alpha)^{1/3}]}$	$[1-(1-\alpha)^{1/3}]^2$
Three dimensional diffusion (Ginstling-Brouhnstein Eq.)	D_3	$\frac{3}{2[(1-\alpha)^{-1/3}-1]}$	$1-\frac{2\alpha}{3}-(1-\alpha)^{2/3}$
Nucleation & Growth (Johnson-Mehl-Avrami Eq.)	A_m m = 1,2,3,4	$m(1-\alpha)[-\ln(1-\alpha)]^{1-1/m}$	$[-\ln(1-\alpha)]^{1/m}$

Empirical Kinetic Model Function

The irregularly shaped sample particles and reaction interfaces for many real processes are apparently different from the idealized $f(\alpha)$ functions as formulated in Table I. In these cases we have to consider irregular shapes of reacting bodies, polydispersity, shielding and overlapping effects of phases involved in the process etc. From this point of view it would be useful to find an empirical kinetic model function containing the smallest possible number of constants so that there is some flexibility sufficient for describing real DSC data as closely as possible[1].

Such empirical kinetic model was proposed by Šesták and Berggren[2] in the following form

$$f(\alpha) = \alpha^M(1-\alpha)^N[-\ln(1-\alpha)]^R \tag{4}$$

It was believed[1,2] that this kinetic model, containing three exponential terms, could describe any non-isothermal kinetic data. Further mathematical analysis[3] has shown that no more than two kinetic exponents are necessary, which led to the so-called Šesták-Berggren kinetic model SB. It is usually written as

$$f(\alpha) = \alpha^M(1-\alpha)^N \tag{5}$$

The exponents M and N are taken as kinetic parameters which describe the measured non-isothermal DSC data. It was shown later[4] that physically

acceptable values of the kinetic exponent M for the SB model are confined to the interval $0 < M < 1$. If the exponent M is set equal to zero, the remaining exponent N is then called reaction order and corresponds to the so-called reaction order model RO. This model is formally identical with the R_n model where non-integral exponent is taken as the value corresponding to fractal dimension[5]. The Johnson-Mehl-Avrami kinetic model A_m can also be easily formalized with non-integral dimension[6] as an empirical JMA model. For the diffusion controlled reaction, Ozao and Ochiai[7] derived a simple description for diffusion models with non-integral exponents by assuming the proportionality of the rate of volume shrinkage to the amount of diffused substance and the concentration gradient along the direction of diffusion. All these models can be understood in terms of the accommodation function introduced by Šesták[5]. In this case the heterogeneous kinetics is assumed to be a distorted case of a simpler homogeneous kinetics. The accommodation function then expreses a deviation of the more complex reaction mechanism from the ideal case. Table II lists the most frequently used empirical kinetic model functions for these cases.

Table II Empirical kinetic model functions $f(\alpha)$ and their integral form $g(\alpha)$

Model	Symbol	$f(\alpha)$	$g(\alpha)$
Reaction order	RO $n \neq 1$	$(1-\alpha)^n$	$\frac{1-(1-\alpha)^{1-n}}{1-n}$
Johnson-Mehl-Avrami	JMA $0.5 < m < 4$	$m(1-\alpha)[-\ln(1-\alpha)]^{1-1/m}$	$[-\ln(1-\alpha)]^{1/m}$
Šesták-Berggren	SB $0 < M < 1$	$\alpha^M(1-\alpha)^N$	no analytical form

The concept of the empirical kinetic model function led to the idea that such an empirical kinetic model as the SB function would provide a general expression for all kinetic models. Recently it was shown[8,9] that such approach in some cases can cause distortion of the Arrhenius parameters because of their mutual correlation. This problem of the so-called "apparent" kinetic models is analyzed in the following section.

The Correlation of Kinetic Parameters

As the rate constant is characteristic of the $f(\alpha)$ assumed, the Arrhenius parameters are correlated with $f(\alpha)$. This correlation can be expressed by the equation following from the condition for the maximum of DSC peak

$$\ln A = -\frac{\beta x_p}{T_p f'(\alpha_p)} + \frac{1}{RT_p}E \qquad (6)$$

where β is heating rate and symbols with subscript p refer to the maximum of DSC peak. Two terms in brackets can be taken for constants for particular non-isothermal DSC data. Any change in the activation energy is therefore "compensated"-by the change in $\ln A$ as expressed by Eq. (6).

As a consequence of the mutual correlation of the Arrhenius parameters, any DSC curve can be described by an apparent kinetic model instead of the appropriate one[9-11] for a certain value of apparent activation energy E_a. The ratio of the apparent and true activation energies E_a/E can be expressed for the apparent RO(n_a) model by the following equation[9,11]

$$\frac{E_a}{E} = -\frac{f(\alpha_p)}{f'(\alpha_p)} \frac{n_a}{1-\alpha_p} \tag{7}$$

where α_p is the degree of conversion at the maximum of DSC peak and n_a is an apparent kinetic exponent of the apparent RO model. The value of n_a is characteristic of the true kinetic model (see Table III) but α_p depends also on x_p (reduced activation energy at the maximum of DSC peak). It can easily be shown that the value of E_a/E slightly increases with x_p for diffusion models (i.e. D_2, D_3 and D_4) and decreases for the A_m model[9]. The limiting values of E_a/E ratio for large x_p are summarized in Table III.

Table III The values of apparent kinetic parameters for the RO model

Model	n_a	E_a/E (for $x_p \to \infty$)
A_m	1	m
D_2	0.269	0.483
D_3	0.666	0.5
D_4	0.420	0.495

The ratio of the apparent and true activation energy can be expressed for the SB model in the following form[9]

$$\frac{E_a}{A} = -\frac{f(\alpha_p)}{f'(\alpha_p)} \left(\frac{N_a}{1-\alpha_p} - \frac{M_a}{\alpha_p} \right) \tag{8}$$

It should be stressed that any change in apparent activation energy leads to different values of kinetic exponents N_a and M_a. Therefore these two apparent kinetic exponents are mutually interdependent. A characteristic N_a vs. M_a dependence can be found for each true kinetic model as shown in Fig.1.

Nevertheless, it can be seen that that these plots are identical for the D_3 and R_3 models. There is also one common curve corresponding to the A_m model, regardless of the value of the true kinetic exponent m. Similar behaviour was observed also for other master plots[12,13].

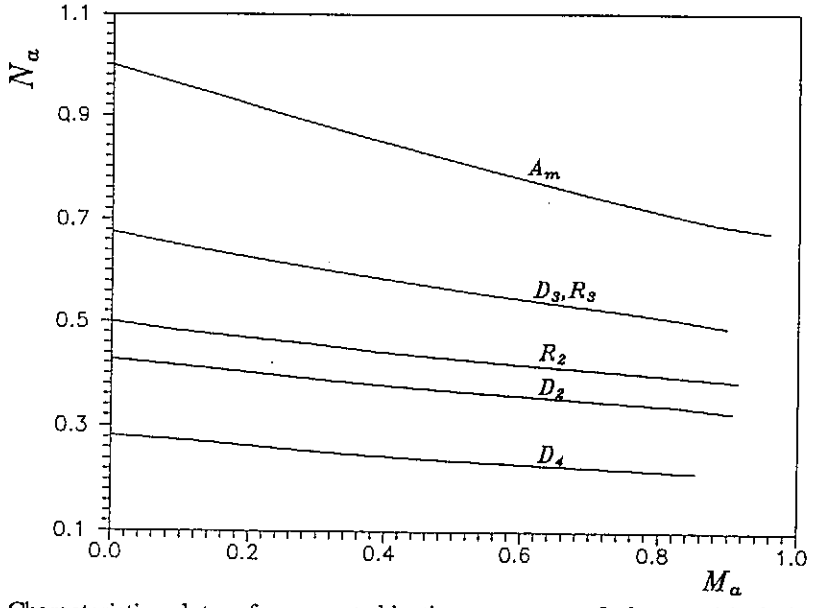

Fig. 1 Characteristic plots of apparent kinetic exponents of the empirical SB model corresponding to the D_2, D_3, D_4, R_2, R_3 and A_m kinetic models

It is clear that any DSC curve can be interpreted within the scope of several apparent kinetic models by simply varying the apparent activation energy. This problem is inherent in the kinetic equation as introduced by Eq. (1). From this point of view, it seems that the methods of kinetic analysis attempting to evaluate all the kinetic parameters from only one experimental DSC curve are rather questionable. We have to realize that this problem cannot be solved, when even not using the most sophisticated multiple linear regression or non-linear regression algorithms, unless the value of the activation energy is known *a priori*. On the other hand, the flexibility of the empirical kinetic models allows the description of very complicated heterogeneous processes where simple kinetic models can hardly be applied.

The correlation of the kinetic parameters with the apparent kinetic models does not allow to perform correctly the kinetic analysis using only one DSC curve. This problem can be solved, however, if the true activation energy is known. Then the most probable kinetic model can be determined and subsequently the preexponential term is calculated. It should be stressed, therefore, that the true value of activation energy is extremely important for any reliable kinetic analysis of non-isothermal DSC data. The method of kinetic analysis is described in the following section.

From the above discussion of correlation of kinetic parameters it follows that the value of true activation energy is important for kinetic analysis at non-isothermal conditions. As a first step in kinetic analysis of non-isothermal DSC data it is suitable to determine the value of activation energy. The calculation of activation energy is based on multiple scan methods where several measurements at different heating rates are required. One of the most typical of these is the Kissinger method[14] based on the equation derived from the condition for the maximum rate on a DSC curve (see above). A very similar method of calculation is the Ozawa method[15]. An alternative calculation procedure is based on the isoconversional method like the Ozawa-Flynn-Wall method[15,16] and the extended Friedman method[17,18]. These methods allow to check the invariance of activation energy with respect to fractional conversion α which is one of the basic assumptions in the kinetic analysis[19].

Friedman method follows from logarithmic form of Eq. (3)

$$\ln\phi = \ln[\Delta HAf(\alpha)] - \frac{E}{RT} \tag{9}$$

The slope of the $\ln\phi$ versus $1/T$ dependence for a given value of α gives the activation energy. This method can successfully be used even if the programmed temperature condition was distorted by the self-cooling and/or self-heating which may occur in the case of heat-flux DSC technique[20].

Once the activation energy has been determined we can find the kinetic model which best describes a measured set of DSC data. It was shown[21] that for this purpose it is useful to define two special functions $y(\alpha)$ and $z(\alpha)$ which can easily be obtained by simple transformation of experimental DSC data

$$y(\alpha) = \phi e^{E/RT} \tag{10}$$

$$z(\alpha) = \phi T^2 \tag{11}$$

In the following part we would like to analyze mathematical properties of these functions from the point of view of kinetic model determination.

By combining the Eqns (3) and (10) the $y(\alpha)$ function can be written as

$$y(\alpha) = \phi e^{x} = \Delta HA f(\alpha) \tag{12}$$

The $y(\alpha)$ function is proportional to $f(x)$ function and, therefore, characteristic of a given kinetic model as shown in Fig. 2. Hence, it can be used as a diagnostic tool for the kinetic model determination. The mathematical condition for the maximum of the $y(\alpha)$ function can be written as

$$f'(\alpha) = \frac{df(\alpha)}{d\alpha} = 0 \tag{13}$$

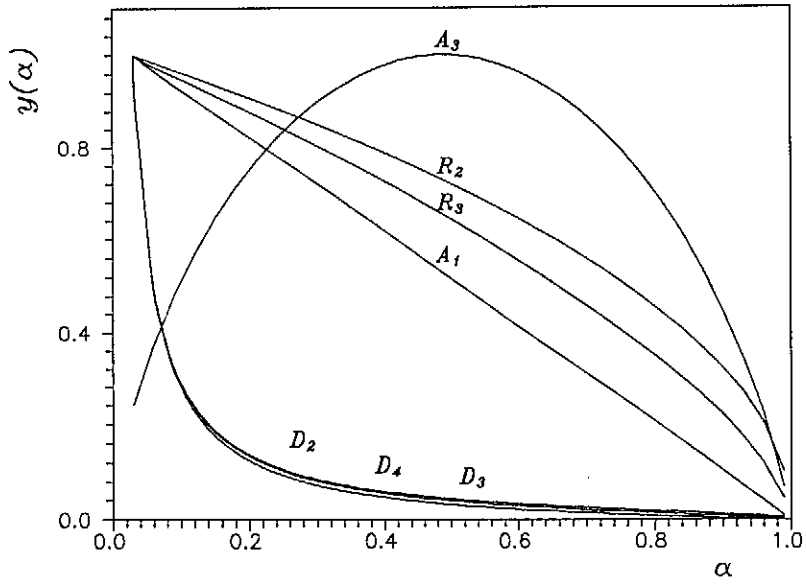

Fig. 2 Typical shapes of the $y(\alpha)$ function for several kinetic models

Comparing Eq. (13) with the $f'(\alpha)$ functions for basic kinetic models, one can find that the D_2, D_3, D_4 and R_n models have a maximum at $\alpha_M = 0$. On the other hand, the empirical kinetic models JMA and SB have a maximum in the interval $0 < \alpha_M < \alpha_p$. The condition for the maximum of the $y(\alpha)$ function for the JMA model is represented as

$$\alpha_M = 1 - e^{\frac{1-m}{m}} \tag{14}$$

and for the SM model as

$$\alpha_M = \frac{M}{M+N} \tag{15}$$

It should be stressed that the position of this maximum is strongly influenced by the value of activation energy. Hence the true activation energy is decisive for a reliable determination of the kinetic model.

Similarly we can discuss the mathematical properties of the $z(\alpha)$ function. The integration of Eq. (1) in non-isothermal conditions for constant heating rate β gives

$$g(\alpha) = \int_0^{\alpha} \frac{d\alpha}{f(\alpha)} = \frac{AE}{\beta R} e^{-x}\left[\frac{\pi(x)}{x}\right] \tag{16}$$

where $\pi(x)$ is an approximation of the temperature integral which has to be introduced because the exponential term in Eq. (1) cannot be integrated

analytically. There are many approximate expressions of the $\pi(x)$ function[1]. According to our experience, the 4th rational expression of Senum and Yang[22] gives sufficiently accurate results

$$\pi(x) = \frac{x^3 + 18x^2 + 88x + 96}{x^4 + 20x^3 + 120x^2 + 240x + 120} \tag{17}$$

By combining Eqns (3) and (16) the $z(\alpha)$ equation is obtained

$$z(\alpha) = \phi T^2 = \left[\frac{\Delta H T\beta}{\pi(x)}\right] f(\alpha) g(\alpha) \tag{18}$$

The term in the bracket is practically constant and does not depend on α in the temperature range of typical DSC peak. This means that in this particular case the $\pi(x)$ function can be approximated as $\pi(x) \approx 1/x$, which corresponds to its limit for high x values[1]. Differentiation of Eq. (18) with respect to α then gives

$$z'(\alpha) = \frac{\Delta H T\beta}{\pi(x)} [f'(\alpha) g(\alpha) + 1] \tag{19}$$

By setting Eq. (19) equal to zero, the mathematical condition for the maximum of the $z(\alpha)$ function is obtained

$$-f'(\alpha_p^\infty) g(\alpha_p^\infty) = 1 \tag{20}$$

which is fulfilled at a fractional conversion $\alpha = \alpha_p^\infty$. It can easily be shown[21] that this value corresponds to the maximum of a hypothetical DSC peak for $x_p \to \infty$. An important fact is that α_p^∞ does not depend on kinetic parameter E and A. Hence, it has a values typical of the basic kinetic models as summarized in Table IV. In fact these values slightly depend on procedural parameters like heating rate, thermal conductivity and heat capacity of sample etc. The deviation from the values given in Table IV usually does not exceed 3%. While the α_p^∞ value is invariant with respect to kinetic exponent for the JMA model, in the case of other empirical kinetic models it depends on kinetic exponents as shown in Fig. 3.

From the analysis shown above, it is evident that the shape of the $y(\alpha)$ function and parameters α_M, α_p^∞ can be used as a diagnostic tool for the determination of the most suitable kinetic model. The procedure is schematically shown in Fig. 4.

In the case that an empirical kinetic model is found as the most probable description of experimental DSC data it becomes necessary to determine the kinetic exponents. There are some methods developed for this purpose. The kinetic exponent n of the RO model can be calculated iteratively using equation[21]

$$\alpha_p = 1 - \left[1 + \frac{1-n}{n} x_p \pi(x_p)\right]^{\frac{1}{n-1}} \tag{21}$$

Table IV Typical values of the maxima of the $z(\alpha)$ function for basic kinetic models

Model	α_p^∞
R_2	0.750
R_3	0.704
D_2	0.834
D_3	0.704
D_4	0.776
A_m	0.632

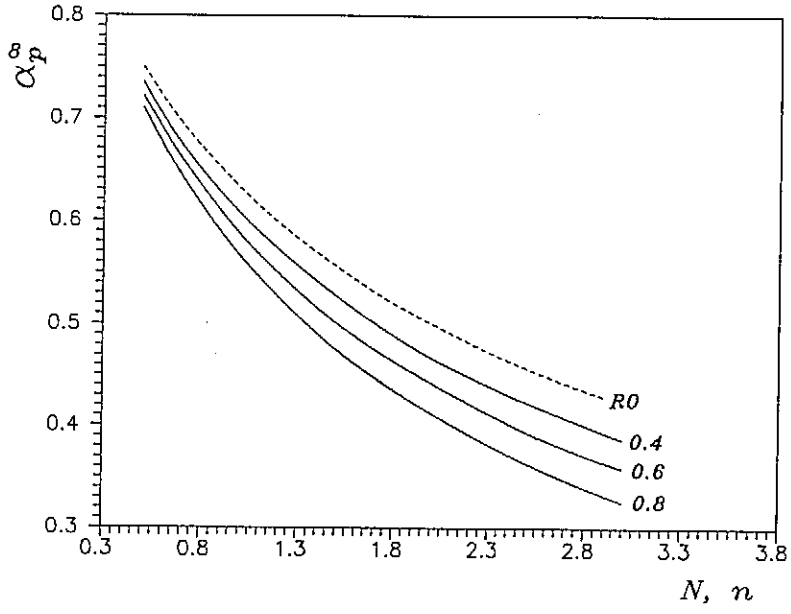

Fig. 3 The dependence of the maximum of the $z(\alpha)$ function α_p^∞ on the kinetic exponent for the RO model (broken line) and the SB model (full lines). The values of the kinetic exponent M are marked by numbers

For the JMA model where $m > 1$, the $y(\alpha)$ function has a maximum at $0 < \alpha_M < \alpha_p$ and the kinetic exponent m is calculated using Eq. (14). For the JMA model where $n \leq 0$m ≤ 0, the $y(\alpha)$ function decreases steadily and the kinetic exponent m can be calculated as

$$m = \frac{1 - x_p \pi(x_p)}{\ln(1 - \alpha_p) + 1} \tag{22}$$

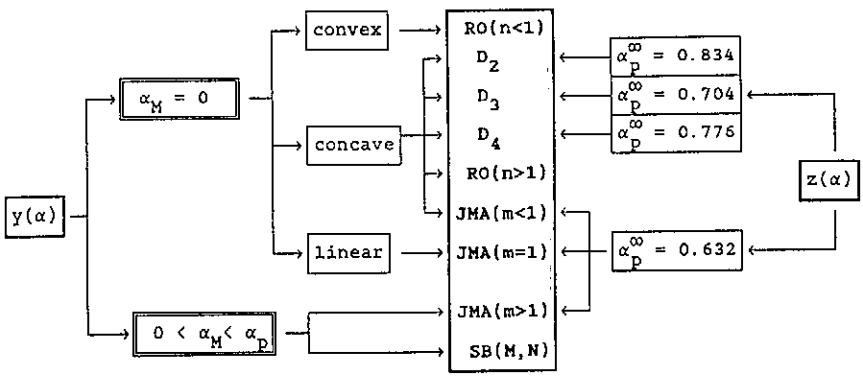

Fig. 4 The kinetic model determination using $y(\alpha)$ and $z(\alpha)$ functions

For the SB model the rearrangement of Eq. (15) gives the ratio of the kinetic exponents $p = M/N$

$$p = \frac{\alpha_M}{1-\alpha_M} \tag{23}$$

Taking the logarithm of Eq. (12) for the SB model we obtain

$$\ln y(\alpha) = \ln[\Delta H A] + N \ln[\alpha^p (1-\alpha)] \tag{24}$$

The kinetic parameter N corresponds to the slope of linear dependence of $\ln[y(\alpha)]$ versus $\ln[\alpha^p(1-\alpha)]$ for). Then the second kinetic exponent is $M = pN$.

Knowing the value of activation energy and the kinetic model, the preexponential term can be calculated using Eq. (6). As in the case of activation energy (see above) also the preexponential factor should be independent of α. This condition can easily be verified. Rearrangement of Eq. (12) gives

$$A = \frac{1}{\Delta H} \frac{\phi e^{\frac{E}{RT}}}{f(\alpha)} \tag{25}$$

As the value of enthalpy change ΔH is directly obtained from DSC data, the value of A at different α can be calculated allowing to check the invariance of A with respect to fractional conversion α.

Based on the method of kinetic analysis described above a software package called TA-system was developed for PC/AT. This software is very simple to use and it features flexible and interactive graphics capabilities which will present the results in a optimal way as required by the user. The experimental DSC data from the most DSC instruments available on the market (Perkin-Elmer, Mettler, Setaram, Rigaku) can be directly imported and processed by this software.

The first step in any non-isothermal data analysis is calculation of the activation energy and verification of its invariance with respect to α. This value is used to calculate the $y(\alpha)$ and $z(\alpha)$ functions necessary for the kinetic model determination. Then the preexponential term and kinetic exponents (for empirical kinetic models) are calculated . This procedure is repeated for all heating rates. If the mechanism of the process does not change during a DSC experiment, it is reasonable to expect that it is possible to find the same kinetic parameters for different heating rates. The consistency of the kinetic model and calculated kinetic parameters is assessed by comparing both experimental and calculated DSC curves for different heating rates. Calculated kinetic parameters allow the prediction of the behaviour of the studied system under isothermal or other selected conditions as demonstrated below for selected examples of non-isothermal kinetics.

All figures presented in this paper were generated by the TA-system and then plotted by GRAPHER (Golden Software Inc., U.S.A.).

Curing Reaction of an Epoxy Resin

The physical properties of a thermosetting system are dependent on the extent of cure, which depends on the curing conditions, and the time and temperature of cure. For this reason, the kinetic characterization of a curing reaction is important in order to obtain thermosets with controlled physical properties and for establishing the optimum curing conditions. The DSC technique has been found to be a useful tool to study exothermic curing reaction[24,25]. Nevertheless, some discrepancies were observed between the kinetic data obtained from isothermal and non-isothermal experiments[26, 27]. In this section we would like to show that if the kinetic analysis is performed correctly then the kinetic parameters obtained from non-isothermal experiments allow us to get a good prediction for isothermal data[28].

A commercial epoxy resin based on diglycidyl ether of bisphenol A (CIBA GEIGY Araldite CY225) with an epoxy equivalent of 188 g equiv^{-1} and Hoepler viscosity of 11.54 Pa s was used in this study. A hardener derived from methyl tetrahydrophtalic anhydride with an accelerator (CIBA GEIGY HY225) was used to cure the resin. The resin and hardener were mixed in a weight ratio

of 10:8. The mixture was stirred at room temperature for 20 min and then degassed in a vacuum chamber at room temperature for 15 min. Samples of about 10mg were encapsulated in aluminium DSC pans and measured using a Mettler TA4000 thermoanalyzer coupled with a low temperature DSC30 module. Non-isothermal DSC curves were obtained with selected heating rates (2.5, 5, 10 and 20 K/min) in the range from -80 °C to 280 °C. Isothermal DSC curves at curing temperatures of 120 - 140 °C were recorded directly in the calorimeter. The isothermal experiments below 120 °C give very low level of heat flow which does not allow to get a sufficiently accurate result. In these cases the residual enthalpy of curing (ΔH_{res}) was measured using samples scanned at 10 K/min after isothermal treatment in thermostatic bath. The fractional conversion of the curing process was then calculated using the following equation[29]

$$\alpha = \frac{\Delta H - \Delta H_{res}}{\Delta H} \tag{26}$$

where ΔH is the total enthalpy of curing corresponding to the "as mixed" sample without previous curing treatment determined by non-isothermal DSC method : $-\Delta H = 298 \pm 3$ J g^{-1}. This procedure is referred to as "the residual enthalpy method" here.

The values of the activation energy calculated by the Friedman method (see above) for different values of the fractional conversion are plotted in Fig. 5. The value of activation energy is practically constant in the interval $0.3 < \alpha < 0.7$. This mean value of the activation energy $E = 74 \pm 1$ kJ mol^{-1} (shown by broken line), was used for kinetic calculations. The standard deviation of the activation energy is lower than 2%. The calculated activation energy agrees with values for the epoxy-anhydride system reported by Fava[30] (74.6 kJ mol^{-1}) and Zukas[31] (75.6 kJ mol^{-1}).

The measured DSC data were converted to $y(\alpha)$ and $z(\alpha)$ functions using Eqs (10) and (11). These functions normalized within the $\langle 0, 1 \rangle$ interval are plotted in Fig. 6 for different heating rates. It is clear that all these functions are independent of the heating rate and give well defined maxima

$$\alpha_M = 0.26 \pm 0.02 \text{ and } \alpha_p^{\infty} = 0.53 \pm 0.01$$

Comparing these results with the scheme shown in Fig. 4, the kinetic model should correspond to the SB model. The calculated kinetic parameters for this model are

$$M = 0.49 \pm 0.04, \; N = 1.42 \pm 0.02 \text{ and } \ln[A/\text{s}^{-1}] = 15.9 \pm 0.1$$

Experimental DSC data (points) and curves calculated using Eq. (3) and these kinetic parameters (full lines) are compared in Fig. 7. It is evident that two parametric empirical SB models give a good description of non-isothermal DSC data for curing reaction of epoxy-anhydride system.

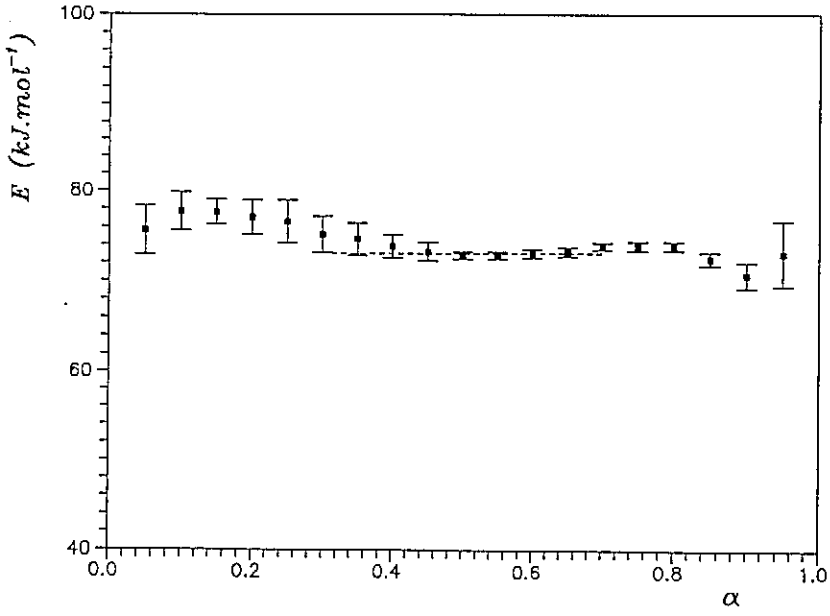

Fig. 5 The values of the activation energy as a function of fractional conversion for the curing reaction of epoxy resin calculated by the Friedman method

It is interesting to compare the kinetic results obtained from non-isothermal data and isothermal experiments at a given temperature of curing T_c. After integration of Eq. (1) at isothermal conditions, the following expression is obtained

$$g(\alpha) = Ate^{-x} \tag{27}$$

Taking the average kinetic parameters corresponding to non-isothermal data, we can calculate theoretical $\alpha - t$ curves because both A and $x = E/RT_c$ are constants. These calculated curves (full lines) are compared with experimental isothermal data (points) in Fig. 8. It can be seen that the experimental and calculated curves are practically identical for curing temperatures of 140 °C and 130 °C where the kinetics of curing process is controlled purely by chemical reaction. For the temperature of 120 °C there is small deviation observed for times longer than 30 min. This discrepancy becomes more important when the isothermal curing temperature T_c is lower than the glass transition temperature of completely cured epoxy resin (i.e. about 109 °C). It seems that the curing progresses through two different stages. The first stage is fully controlled by the chemical reactivity of groups; the curing reaction develops in the liquid state. With increasing crosslinking the glass transition temperature T_g of the epoxy system increases until it equals T_c. On reaching this point, the second stage of curing starts. The system vitrifies and the reaction rate decreases considerably until the reaction becomes practically frozen due to the fact that the mobility of the reacting groups becomes very restricted.

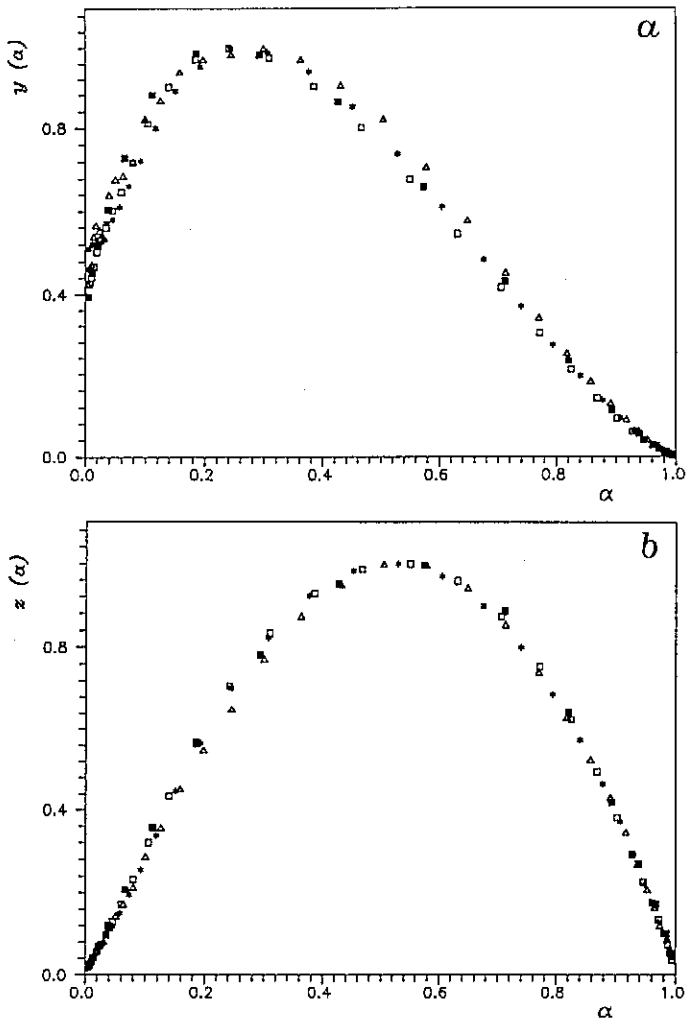

Fig. 6 Transformed DSC data for the suring process of epoxy resin: (a) Normalized $y(\alpha)$ function. (b) Normalized $z(\alpha)$ function. The heating rates are shown by various points: (△) 2.5; (★) 5; (□) 10 and (■) 20 K min^{-1}. The points were calculated from Eqs (10) and (11), respectively

These two stages are evident in Fig .9 where the isothermal $\alpha - t$ curves are shown for temperatures below 120 °C. These isothermal data (points) cannot be measured directly because of the very low heat flow rate and, therefore, they have been constructed by the method of residual enthalpy (see above). There is relatively good agreement between experimental points and predicted isotherms (full lines) for low α. However, later the system reaches the glassy state and the kinetics becomes controlled by diffusion[29,32-34]. The slow segmental motions are the only permitted ones and the measured $\alpha - t$ curves differ from the predicted ones. The extremely high viscosity of the system prevents full conversion of the

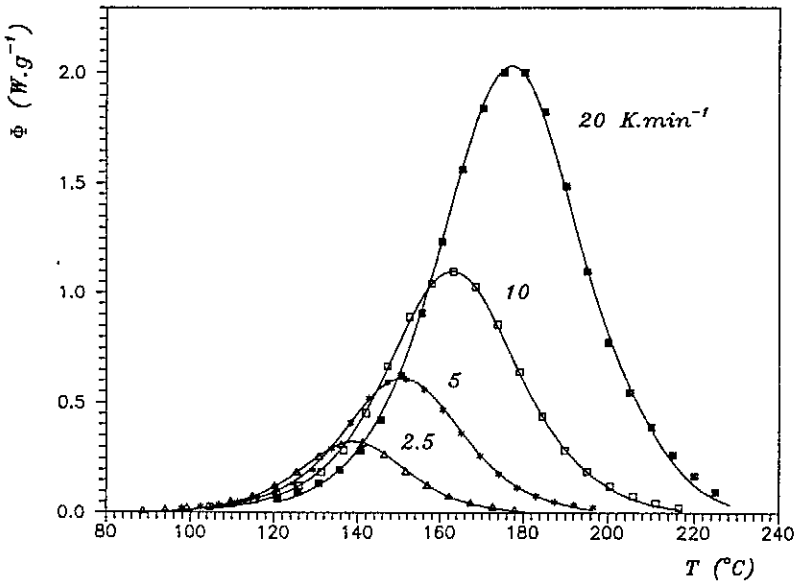

Fig. 7 Experimental (points) and calculated (full lines) DSC curves corresponding to the curing process of epoxy resin at various heating rates. The symbols used are as in Fig. 6

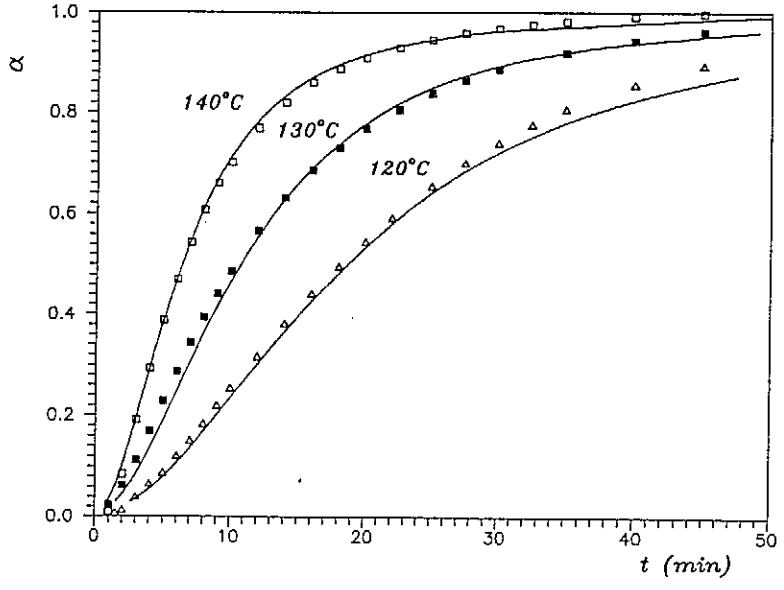

Fig. 8 Comparison between the experimental (points) and calculated isothermal time-transformation curves for a curing process of epoxy resin. The full lines were calculated using Eq. (27) for the kinetic parameters obtained from non-isothermal DSC data

chemical reaction and the degree of conversion tends to have a practically constant limiting value of fractional conversion, even for very large time scales.

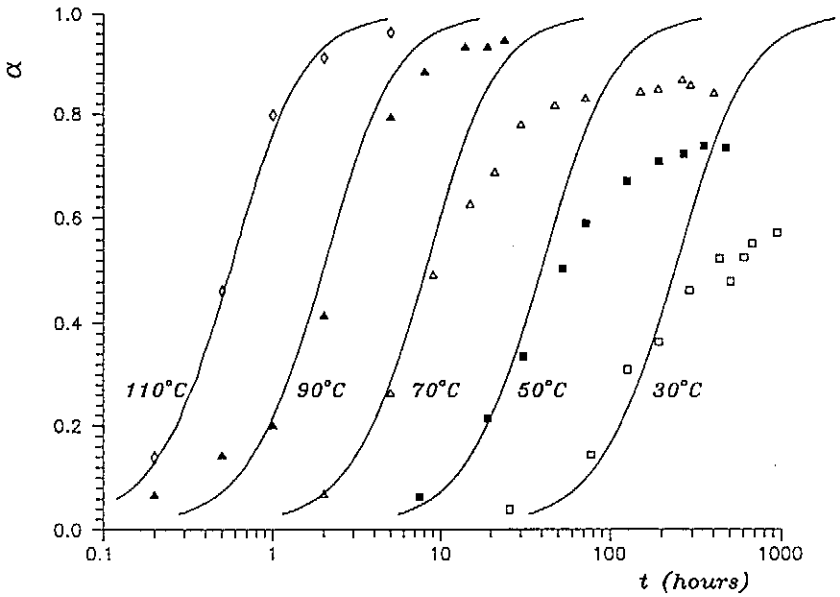

Fig. 9 Comparison between the experimental and calculated isothermal time-transformation curves for curing process of epoxy resin. The points were determined from the residual enthalpy of partially cured resins. The full lines were calculated using Eq. (27) for the kinetic parameters obtained from non-isothermal DSC data

This area of restricted mobility where the vitrification occurs is also shown in the TTT diagram in Fig. 10. This diagram was calculated using the kinetic parameters determined from non-isothermal data. The limiting values for T_g corresponding to the uncured (T_{g0}) and fully cured ($T_{g\infty}$) resin are shown by broken lines. The T_g of a partially cured resin is confined to the range between these limiting values. If curing temperature is lower than $T_{g\infty}$, then the system vitrifies after a certain time. This "vitrification" time depends on the curing temperature[44] and is shown by the dotted line.

It was established that the curing reaction of diglycidyl ether of bisphenol A with methyltetrahydrophtalic anhydride containing an accelerator can be described by a two-parameter SB kinetic model. The kinetic parameters calculated from kinetic analysis of non-isothermal data allow to predict isothermal curves showing a very good agreement with experimental data at curing temperatures above the glass transition temperature. When the vitrification region is reached, a more complex model should be taken into account to describe the curing process controlled not only by chemical reaction.

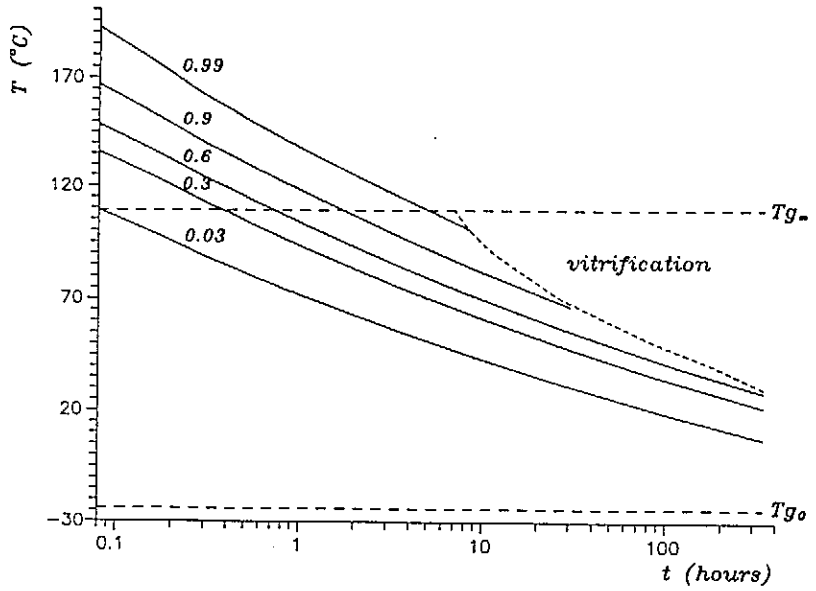

Fig.10 Time-temperature-transformation diagram for a curing process of epoxy resin calculated from Eq, (27) (full lines α = 0.03, 0.3, 0.6, 0.9 0.99). The broken lines show the T_{g0} and $T_{g\infty}$. The dotted line marks the vitrification region where the curing reaction is frozen

Crystallization Kinetics of a Chalcogenide Glass

The study of crystallization processes in glasses is important for better understanding the thermal stability of glasses and also for preparation of glass-ceramic materials with controlled properties. Although the general theory of crystallization transformation kinetics is largely confined to the description of the isothermal conditions, there are many instances where the kinetic behaviour of a system which is heated or cooled through the transformation region is of greater practical importance[35-40]. Non-isothermal experiments can be used e.g. to extend the temperature range of measurements beyond that accessible by isothermal experiments[1,41].

The studied glass of composition $Ge_{0.3}Sb_{1.4}S_{2.7}$ was prepared using germanium and antimony and sulfur with nominal purity 5N. A mixture of these elements was placed in a quartz ampoule which was then evacuated to a pressure of 10^{-4} Pa and sealed. After heat treatment (10h at 900 °C), the ampoule was rapidly quenched in cold water to room temperature. The glassy nature and chemical composition of the prepared sample were checked by X-ray diffraction (XRD) and electron microanalysis, respectively. All the experiments were carried out on bulk or powder (avg. particle size 0.1 μm) samples of about 10 mg in sealed aluminium pans using a Perkin-Elmer DSC7 instrument coupled

with PE7700 Data Station. The measurements were performed at different heating rates (2, 5, 10, 15 and 20 K/min). Only one well defined DSC crystallization peak was observed corresponding to the crystallization of Sb_2S_3 phase as it was confirmed by XRD. The morphology of crystal growth was studied by means of a HITACHI S-5000 Scanning Electron Microscope (SEM).

Bulk Sample

The total crystallization enthalpy for the bulk sample was determined to be $-\Delta H = 56 \pm 1$ J g^{-1}. The values of the activation energy calculated by the Friedman method (see above) for different values of the fractional conversion are plotted in Fig. 11. The value of activation energy is practically constant in the interval of $0.3 < \alpha < 0.7$. The mean value of the activation energy $E = 163 \pm 11$ J mol^{-1} (shown by broken line) was used for kinetic calculations. The standard deviation of the activation energy is less than 10%. The calculated activation energy agrees well with value found by Ryšavá et al.[42,43] (159 - 178 kJ mol^{-1}) by both isothermal and non-isothermal methods.

The measured DSC data were converted to $y(\alpha)$ and $z(\alpha)$ functions using Eqs (10) and (11). These functions normalized within the $\langle 0, 1 \rangle$ interval are plotted in Fig. 12 for different heating rates. It is clear that all these functions are independent of the heating rate and give well defined maxima

$$\alpha_M = 0.45 \pm 0.04 \text{ and } \alpha_p^{\infty} = 0.64 \pm 0.03$$

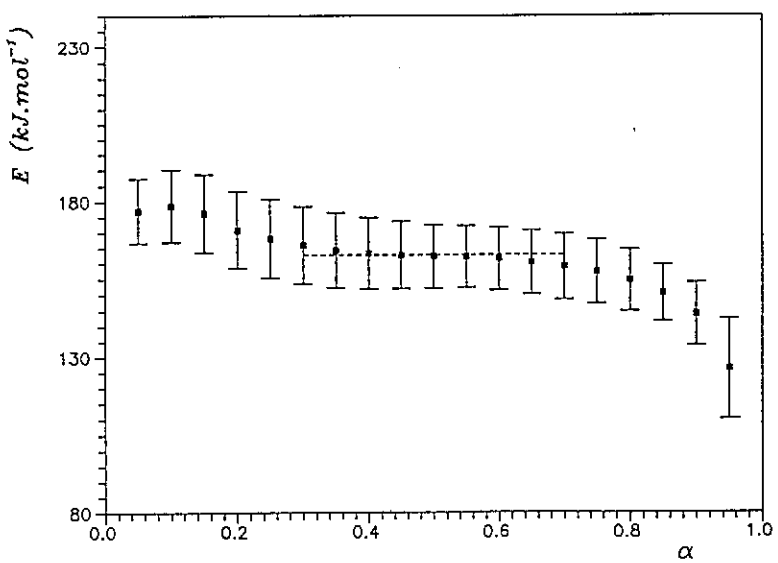

Fig. 11 The values of the activation energy as a function of fractional conversion for the crystallization of bulk of the $Ge_{0.3}Sb_{1.4}S_{2.7}$ glass calculated from the Friedman method

These results suggest that the kinetic model should correspond to the JMA model. The calculated kinetic parameters for this model are

$$m = 3.0 \pm 0.2 \text{ and } \ln[A/s^{-1}] = 24.1 \pm 0.2$$

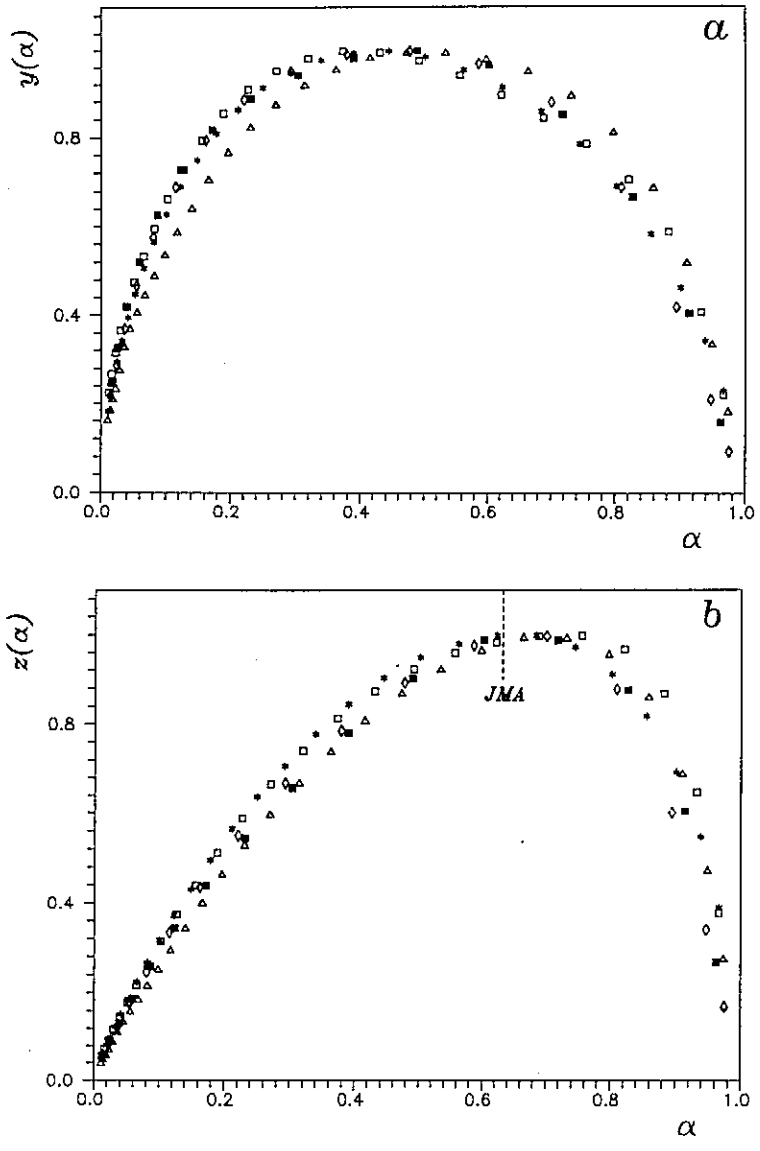

Fig. 12 Transformed DSC data for the crystallization of the $Ge_{0.3}Sb_{1.4}S_{2.7}$ bulk glass: (a) Normalized $y(\alpha)$ function. (b) Normalized $z(\alpha)$ function. The heating rates are shown by various points: (△) 2; (★) 5; (□) 10; (■) 15 and (◇) 20 K min^{-1}. The points were calculated from Eqs (10) and (11), respectively. The maximum of the $z(\alpha)$ function for the JMA model is marked by broken line

Experimental DSC data (points) and curves calculated using Eq. (3) and these kinetic parameters (full lines) are compared in Fig. 13. The kinetic exponent is close to 3 (within the error limits) which is a value typical for a three-dimensional growth after saturation of nucleation sites, i.e. for zero nucleation rate. The three-dimensional growth of Sb_2S_3 was confirmed by SEM microscopic observations[44].

It is evident that the JMA model gives a good description of non-isothermal DSC data for the crystallization process of the $Ge_{0.3}Sb_{1.4}S_{2.7}$ glass. This means that all the important assumptions[45-49] for validity of the JMA model are fulfilled:

(1) Isothermal crystallization conditions
(2) Homogeneous nucleation or heterogeneous nucleation at randomly dispersed second phase particle
(3) Growth rate of new phase is controlled by temperature and is independent of time

It has been shown by Henderson[41] and also by DeBruijn et al.[50] that the validity of the JMA model can be extended to non-isothermal condition if the crystals of a new phase grow from a constant number of nuclei and the nucleation process is completed prior to crystal growth. Strictly speaking, only under these conditions kinetic exponent m corresponds to the dimensionality of crystal growth. Recent computer simulations by Shepilov an Baik[51] revealed that for

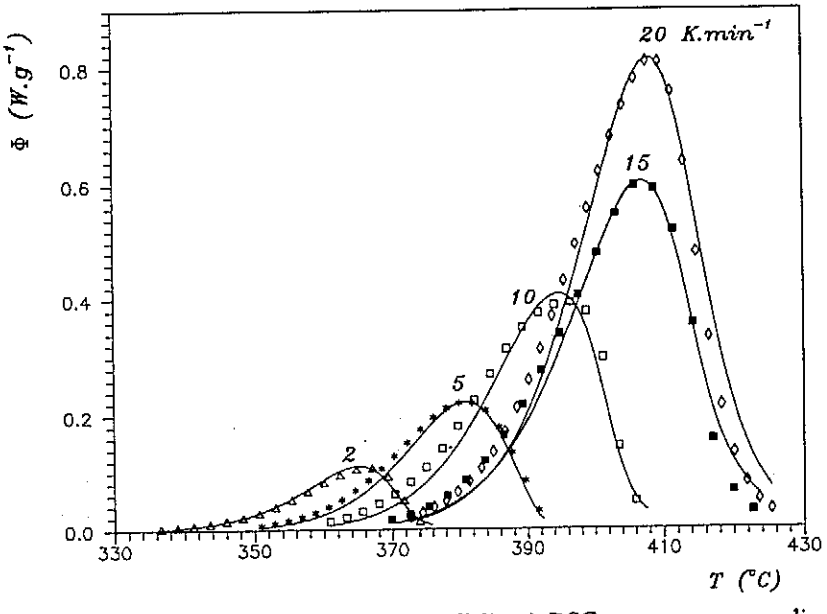

Fig. 13 Experimental (points) and calculated (full lines) DSC curves corresponding to the crystallizatin of the $Ge_{0.3}Sb_{1.4}S_{2.7}$ bulk glass at various heating rates. The symbols used are as in Fig. 12

higher crystal anisotropy the dimensionality of growing crystals cannot unambiguously be determined from the value of kinetic exponent. Therefore, some complementary experiments such as microscopic observation of crystal growth morphology become necessary. It is well known that the DSC measurements reflect mainly the process of crystal growth. It seems, however, that a very good test for the applicability of the JMA equation is the maximum of the $z(\alpha)$ function which should be confined to the interval $\alpha_p^{\infty} \approx 0.632$, as discussed above.

Under these circumstances the JMA model can give a good prediction of the crystallization extent under isothermal conditions. Fig. 14 shows the temperature dependence of a fraction crystallized after 1 hour isothermal annealing. The points were determined by the residual enthalpy method described above (see Eq. (26)) and the full line was calculated using Eq. (27) using kinetic parameters calculated from non-isothermal data. We can conclude that the theoretical JMA model can be used to predict the crystallization kinetics for a bulk sample of the $Ge_{0.3}Sb_{1.4}S_{2.7}$ glass even at isothermal conditions.

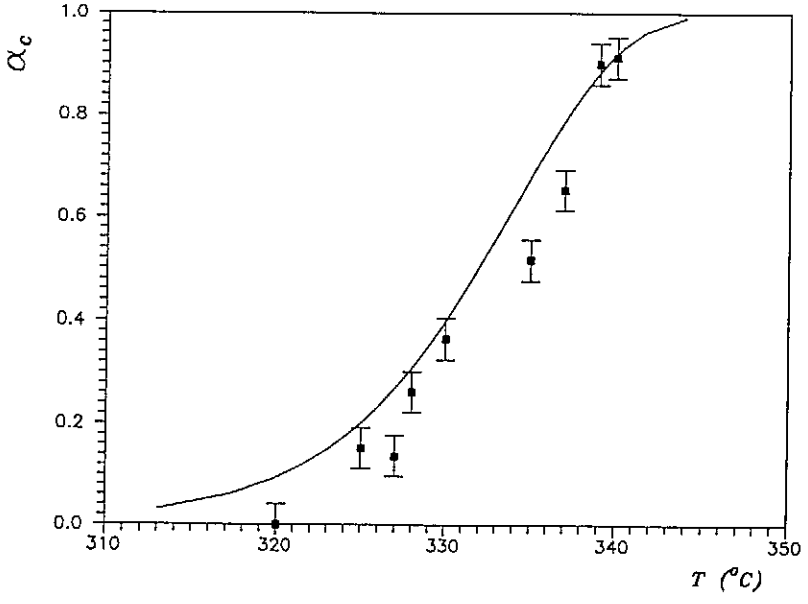

Fig. 14 Comparison between the experimental and calculated temperature-transformation curves for 1 hour annealing of the $Ge_{0.3}Sb_{1.4}S_{2.7}$ bulk glass. The points were determined from the residual enthalpy of partially crystallized glass. The full line was calculated using Eq. (27) for the kinetic parameter obtained from non-isothermal DSC data

Powder Sample

The total crystallization enthalpy for powder sample was determined to be $-\Delta H = 52 \pm 1$ J g^{-1}, which is a lower value than for bulk sample. The mean value of the activation energy determined by the Friedman method is $E = 236 \pm 7$ kJ mol^{-1}. This value is considerably higher than that for bulk sample. It can probably be explained by the influence of higher specific surface of the sample. On the other hand, a powder sample has a better thermal contact with DSC sample pan and, therefore, the activation energy has a lower standard deviation than that for bulk sample.

The measured DSC data were converted to $y(\alpha)$ and $z(\alpha)$ functions and normalized within the $\langle 0, 1 \rangle$ interval are plotted in Fig. 15 for different heating rates. All these functions are independent of the heating rate and give well defined maxima

$$\alpha_M = 0.28 \pm 0.01 \text{ and } \alpha_p^{\infty} = 0.52 \pm 0.01$$

The standard deviations are also lower than for the bulk sample. A good thermal contact is very important for the shape of these functions. As it follows from the α_p^{∞}, value the JMA model cannot be applied in this case (see Fig. 4). It is well known that the heat flow measured by DSC technique corresponds mainly to the macroscopic crystal growth. This process, however, is strongly influenced by the preceding nucleation process and by the concentration and distribution of nuclei in the sample. In the case of homogeneous nucleation the number of nuclei per unit volume is the sum of surface nuclei and bulk nuclei formed during the DSC run. In the powder sample, surface nucleation is dominant due to higher specific surface of the sample, and the number of bulk nuclei created during DSC run is small. It seems, however, that besides this primary nuclei preexisting in the sample there is probably a secondary nucleation process[40] taking place during the macroscopic crystal growth. Therefore, the site saturation condition is no longer fulfilled and as a result the JMA model cannot be applied in the case of powder sample.

In this case the two-parameter SB model can be used for a quantitative description of non-isothermal data. The calculated kinetic parameters for this model are

$$M = 0.44 \pm 0.04, \quad N = 1.1 \pm 0.1 \text{ and } \ln[A/\text{s}^{-1}] = 41.8 \pm 0.1$$

The experimental DSC data (points) and curves calculated using Eq. (3) and these kinetic parameters (full lines) are compared in Fig. 16. It is clear that the SB model gives sufficiently accurate description of non-isothermal data. Nevertheless, the description at isothermal conditions is not good and there is a relatively large discrepancy in Fig. 17 between experimental data (points) obtained by the residual enthalpy method (for 1h isothermal annealing) and theoretical curve calculated using Eq. (27). This discrepancy decreases for higher values of fraction crystallized. It is still not clear how to explain this result. The

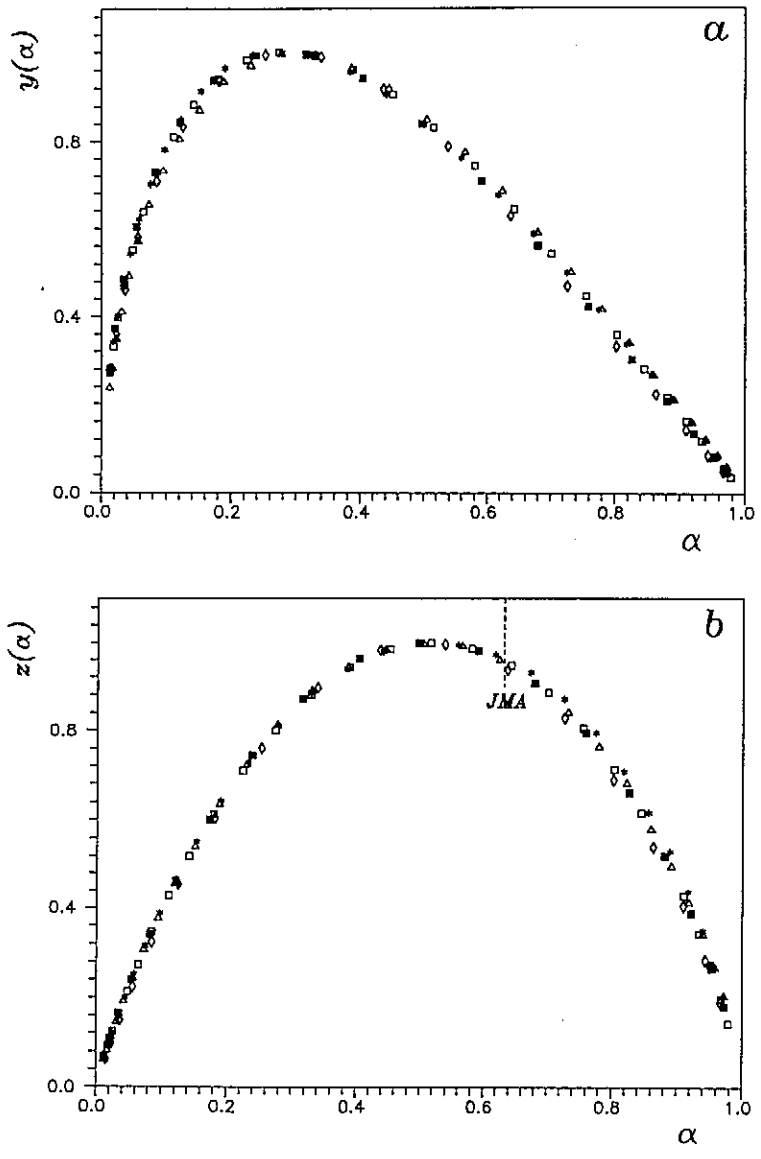

Fig.15 Transformed DSC data for the crystallization of the $Ge_{0.3}Sb_{1.4}S_{2.7}$ powder glass: (a) Normalized $y(\alpha)$ function. (b) Normalized $z(\alpha)$ function. The heating rates are shown by various points: (△) 2; (⋆) 5; (□) 10; (■) 15 and (◇) 20 K min^{-1}. The points were calculated from Eqs (10) and (11), respectively. The maximum of the $z(\alpha)$ function for the JMA model is marked by broken line

microscopic observation found no considerable differences between morphology of crystal growth in bulk and powder sample of the $Ge_{0.3}Sb_{1.4}S_{2.7}$ glass. Hence, it seems that the difference in the crystallization behaviour of bulk and powder

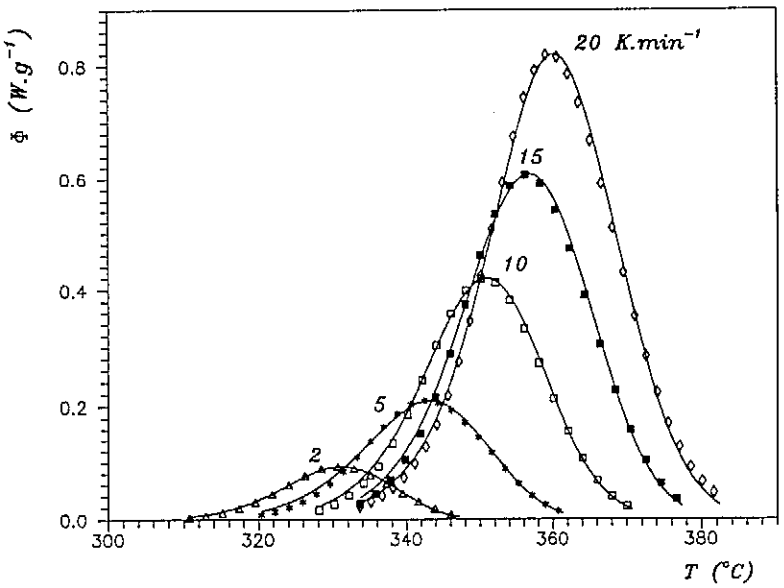

Fig. 16 Experimental (points) and calculated (full lines) DSC curves corresponding to the crystallization of the $Ge_{0.3}Sb_{1.4}S_{2.7}$ powder glass at various heating rates. The symbols used are as in Fig. 15

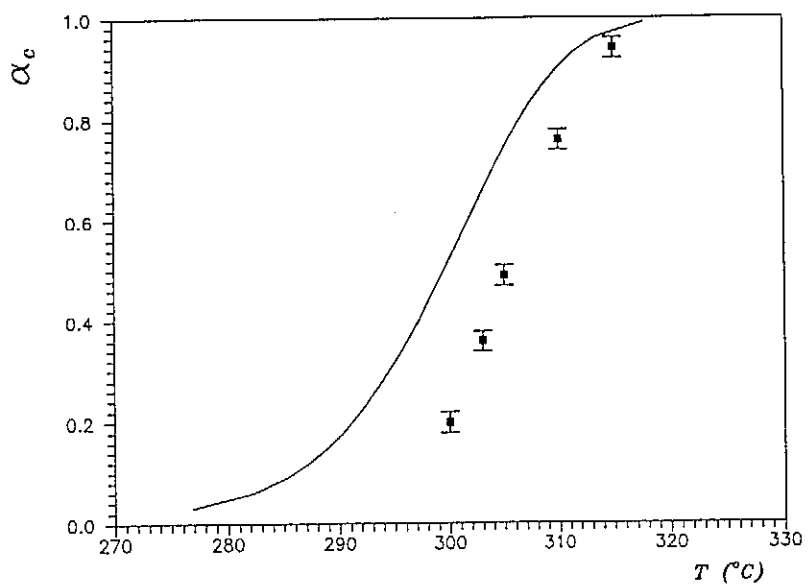

Fig. 17 Comparison between the experimental and calculated temperature-transformation curves for 1 hour annealing of the $Ge_{0.3}Sb_{1.4}S_{2.7}$ powder glass. The points were determined from the residual enthalpy of partially crystallized glass. The full line was calculated from Eq. (27) for the kinetic parameters obtained from non-isothermal DSC data

samples lies more in the nucleation process. It is also possible to assume that there is a secondary nucleation, especially during crystal growth phase. We believe that this problem could be solved by direct observation on partially nucleated samples using e.g. High Resolution Transmission Electron Microscopy.

It was found that the sample specific surface has an important influence on the crystallization kinetics of the $Ge_{0.3}Sb_{1.4}S_{2.7}$ glass. The DSC crystallization data for bulk sample can be described by the JMA model corresponding to three dimensional crystal growth. This model gives a very good description also for crystallization under isothermal conditions. On the other hand, the DSC crystallization data for powder sample cannot be described within the JMA model, and the empirical SB model has to be used. Although the SB model gives a good quantitative description of non-isothermal data, it fails in the case of isothermal conditions. It seems that the condition of site saturation is not fulfilled in this case and that there is probably a secondary nucleation process taking place during macroscopic crystal growth. Nevertheless, this process should be confirmed by further microscopic study.

Crystallization Kinetics of Zirconia Gel

Zirconia ceramics are considered one of the most promising materials for advanced technologies because of their excellent mechanical properties such as fracture toughness, strength, and hardness[52]. They can be fabricated by sintering superfine zirconia powders processed by drying of the gel precipitated from solutions of zirconia salts[53]. The zirconia gel dried at temperatures below 300 °C is amorphous and at higher temperatures it crystallizes and a metastable tetragonal ZrO_2 phase is formed[54]. The kinetics of crystal growth in amorphous zirconia gels is very important for final properties of the ceramics. Although crystallization studies of amorphous zirconia have been undertaken by a number of investigators[55-58], such studies have been confined mainly to a simple description of the crystallization process. As far as we know, no attempt has been made to describe the crystallization process quantitatively.

Zirconia gel sample precipitated from 0.1M solution of $ZrOCl_2.8H_2O$ with ammonia was washed repeatedly with distilled water until the wash water contained no Cl^-, then partially dried 48 hours in vacuum at room temperature. The partially dried sample still contained about 14% of water. Amorphous nature of the prepared zirconia sample was confirmed by XRD and electron diffraction. All the experiments were carried out on pulverized samples of about 10 mg in sealed aluminium pans using a Perkin-Elmer DSC7 instrument coupled with PE7700 Data Station. The measurements were performed at different heating rates (2, 5, 10, 15 and 20 K/min). Only one well defined DSC crystallization peak was observed corresponding to the crystallization of tetragonal ZrO_2 phase ($P4_2/nmc$, a = 3.598 Å, c = 5.152 Å), as it was

confirmed by XRD. Selected area electron diffraction and High Resolution Transmission Electron Microscopy (HRTEM) of partially crystallized samples were carried out on a HITACHI H-1500 microscope operated at 800 kV.

The total crystallization enthalpy of the zirconia gel was determined to be $-\Delta H = 157 \pm 4$ J g^{-1}. The crystallization enthalpy is close to the values published earlier[55,59]. The values of the activation energy calculated by the extended Friedman method (see above) for different values of the fractional conversion are plotted in Fig. 18. The value of activation energy is practically constant in the interval of $0.3 < \alpha < 0.7$. The mean value of the activation energy $E = 233 \pm 10$ kJ mol^{-1} (shown by broken line), was used for kinetic calculations. The standard deviation of the activation energy is less than 5%.

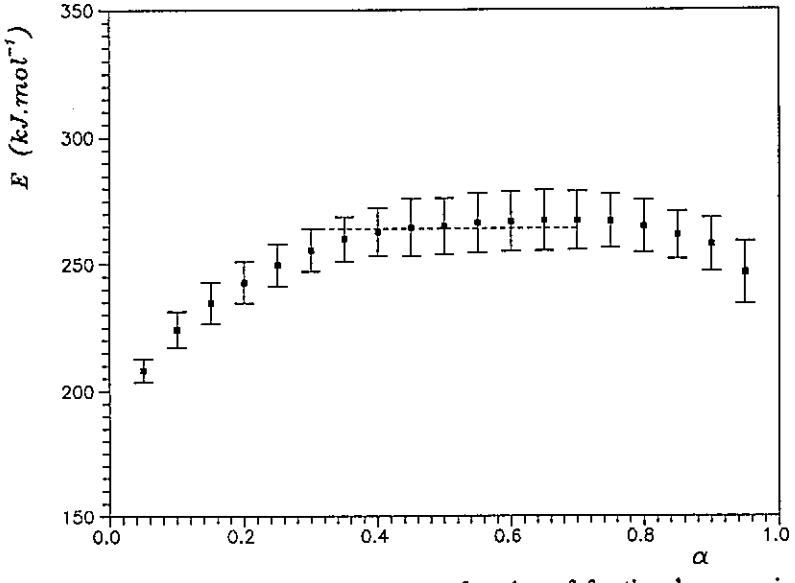

Fig. 18 The values of the activation energy as a function of fractional conversion for the crystallization of dried zirconia gel calculated by the Friedman method

The measured DSC data were converted to $y(\alpha)$ and $z(\alpha)$ functions using Eqs (10) and (11). These functions normalized within the $\langle 0, 1 \rangle$ interval are plotted in Fig. 19 for different heating rates. It is clear that all these functions are independent of the heating rate and give well defined maxima

$$\alpha_M = 0.30 \pm 0.02 \quad \text{and} \quad \alpha_p^{\infty} = 0.36 \pm 0.02$$

The shape of both $y(\alpha)$ and $z(\alpha)$ functions suggests, however, that the kinetics of crystallization in this case is more complex. The partially dried, polymerized zirconia gel undergoes dehydration and crystallization during heating. Thermogravimetric experiments revealed that nucleation-growth process starts after complete dehydration has taken place. It seems, therefore, that the nucleation process is induced by removal of residual water contained in dry

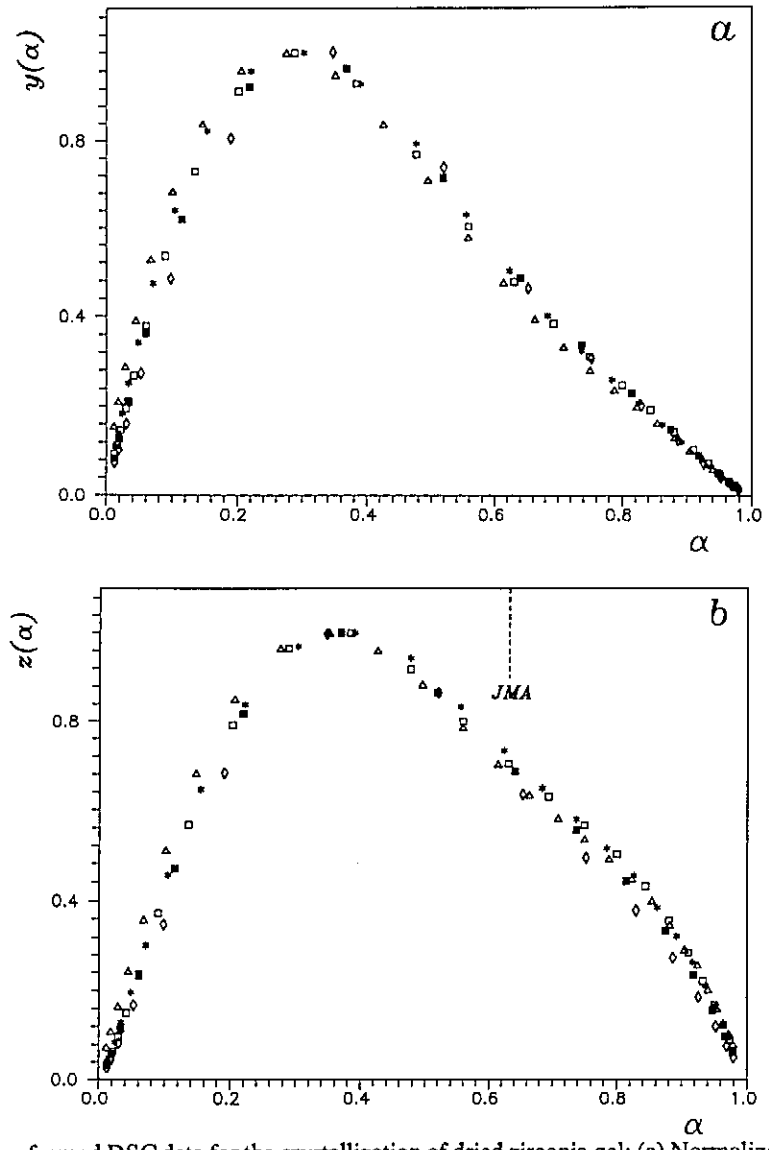

Fig. 19 Transformed DSC data for the crystallization of dried zirconia gel: (a) Normalized $y(\alpha)$ function. (b) Normalized $z(\alpha)$ function. The heating rates are shown by various points: (△) 2; (★) 5; (□) 10; (■) 15 and (◇) 20 K min^{-1}. The points were calculated from Eqs (10) and (11), respectively. The maximum of the $z(\alpha)$ function for the JMA model is marked by broken line

gel[60]. In the case of partially dried zirconia gel there are probably two mutually overlapping processes. One of them is a normal crystal growth process from nuclei induced by dehydration process. This process corresponds to the JMA model and it is demonstrated by a shoulder at $\alpha \approx 0.632$. The growth of tetragonal zirconia phase creates new nuclei centers and, as a consequence of

such overlapping, the maximum of the $z(\alpha)$ function corresponding to the overall process is localized at lower values of α. For partially crystallized zirconia samples this induced secondary nucleation process becomes negligible and the maximum of the $z(\alpha)$ function shifts close to the value characteristic for the JMA model. This explanation is supported by our HRTEM study[61].

Despite the fact that the shape of the $z(\alpha)$ function is rather complicated, the overall crystallization can be described by the empirical SB model for the following kinetic parameters

$$M = 0.58 \pm 0.08, \; N = 1.36 \pm 0.05 \text{ and } \ln[A/s^{-1}] = 41.8 \pm 0.1$$

The experimental DSC data (points) and curves calculated using Eq. (3) and these kinetic parameters (full lines) are compared in Fig. 20. The description of non-isothermal data is not so good as for the curing reaction of epoxy resin or the crystallization of the $Ge_{0.3}Sb_{1.4}S_{2.7}$ glass (see above). However, this model gives a quite good prediction of crystallization extent at isothermal conditions, as it evident from Fig. 21, where experimental data (points) obtained by the residual enthalpy method (for 1h and 3h isothermal annealing) and theoretical curve calculated using Eq. (27) are compared. Nevertheless, this prediction underestimates the crystallization extent for low temperatures where the influence of induced secondary nucleation process is important. For a partially crystallized sample the normal growth process is typical[61], and there is a better accordance with isothermal experimental data. In this case, also non-isothermal

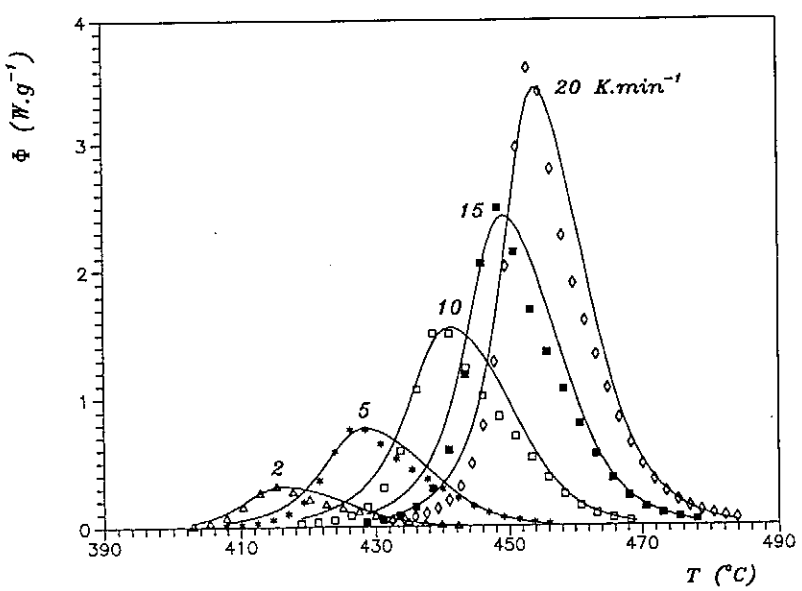

Fig. 20 Experimental (points) and calculated (full lines) DSC curves corresponding to the crystallization of dried zirconia gel at various heating rates. The symbols used are as in Fig. 19

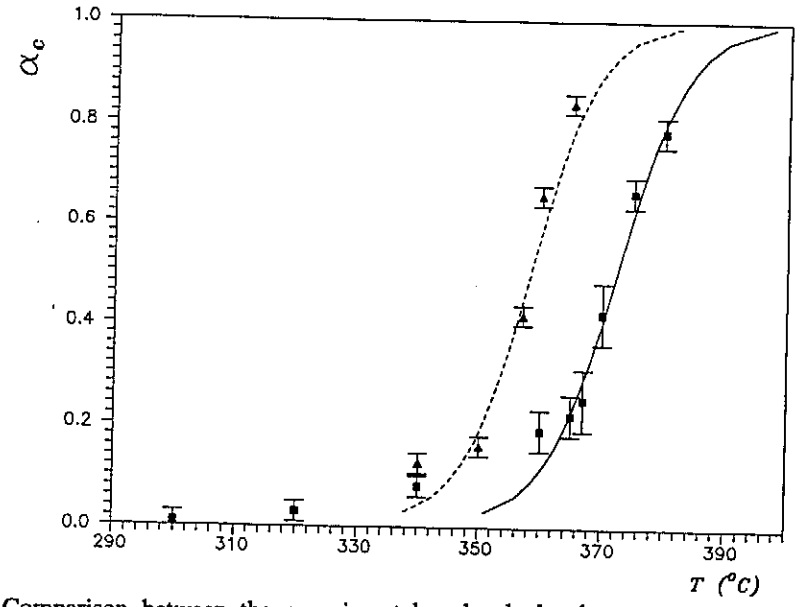

Fig. 21 Comparison between the experimental and calculated temperature-transformation curves for 1 hour annealing (full line) and 3 hours annealing (broken line) of dried zirconia gel. The points were determined from the residual enthalpy of partially crystallized glass. The full line was calculated from Eq. (27) for the kinetic parameters obtained from non-isothermal DSC data

DSC data can be described by the JMA model for kinetic exponent $m = 1$ which indicates that the growth occurs in two dimensions on particles of appreciable initial volume[49].

It was found that the crystallization of partially dried zirconia gel can be described by the empirical SB model. The kinetic parameters calculated from kinetic analysis of non-isothermal data. allow to describe the crystallization kinetics at isothermal conditions. This description is accurate at higher temperatures but there are small deviations in low temperature range. Such deviations are probably caused by an induced secondary nucleation process occurring in partially dried zirconia gels.

Conclusion

It has been shown that the Arrhenius kinetic parameters are mutually correlated. Due to this correlation it is practically impossible to determine all kinetic parameters from one DSC curve. This problem can be solved, however, if the activation energy is determined from several DSC curves measured at different heating rates. Once the activation energy is known, the most suitable kinetic model can be found by means of $y(\alpha)$ and $z(\alpha)$ functions obtained by a simple transformation of DSC data. Based on this procedure, a software package for

kinetic analysis of non-isothermal DSC data was developed. The kinetic parameters calculated from non-isothermal data can be used for a prediction of the reaction rate and reaction extent under isothermal conditions.

Such kinetic analysis is demonstrated for curing reaction of epoxy resin Araldite CY225. It was established that this curing process can be described by the two-parameter empirical Šesták-Berggren kinetic model. This model gives a very good prediction for isothermal curing at temperatures T > 110 °C, i.e. above the glass transition. At lower temperatures the vitrification region is reached and the kinetics is controlled not only by chemical reaction but also by diffusion process. Under these conditions a more complex model should be considered for the description of curing process of the epoxy resin.

It was demonstrated that the Johnson-Mehl-Avrami nucleation-growth model can be used for the description of crystallization process in bulk $Ge_{0.3}Sb_{1.4}S_{2.7}$ glass. The kinetic exponents correspond to three dimensional growth after saturation of nucleation sites. The calculated fraction crystallized at isothermal conditions agrees well with experimental data obtained by means of residual enthalpy method. In the case of powder sample of the same composition the DSC data cannot be described within the Johnson-Mehl-Avrami model and the empirical Šesták-Berggren model has to be used. It seems that the nucleation and growth processes overlap in this case.

The empirical Šesták-Berggren model can also be used for the description of the crystallization of dried zirconia gel. It is assumed that there is probably a secondary nucleation process induced by dehydration process. For partially crystallized zirconia samples the crystallization process can be described by the Johnson-Mehl-Avrami model, which suggests that the secondary nucleation process becomes negligible in this case. This could explain small differences between the calculated and measured reaction extent at low temperatures.

The method proposed in this paper can give the most probable kinetic model and meaningful kinetic parameters. These kinetic parameters are very useful for precise control of reaction extent under isothermal conditions and, therefore, for preparation of materials with defined properties. Nevertheless, it should be pointed out that calculated kinetic parameters (especially kinetic exponents) cannot say anything definitive about the real mechanism of the process under study. From this point of view, attention should be drawn to morphological studies.

References

1. Šesták J.: *Thermophysical Properties of Solids, Their Measurements and Theoretical Thermal Analysis*, Elsevier, Amsterdam 1984.
2. Šesták J., Berggren G.: Thermochim. Acta **3**, 1 (1971).
3. Gorbatchev V.M.: J. Therm. Anal., **18**, 194 (1980).

4. Málek J, Criado J.M, Šesták J, Militký J.: Thermochim. Acta **153**, 429 (1989).
5. Šesták J.: J. Therm. Anal. **36**, 1977 (1990).
6. Málek J.: Thermochim. Acta **138**, 337 (1989).
7. Ozao R, Ochiai M.: J. Ceram. Soc. Jpn. **101**, 263 (1993).
8. Málek J., Criado J.M.: Thermochim. Acta, **175**, 305 (1991).
9. Málek J, Criado J.M.: Thermochim. Acta, **203**, 25 (1992).
10. Criado J.M, Dollimore D., Heal G.R.: Thermochim. Acta **54**, 159 (1982).
11. Koga N., Šesták J., Málek J.: Thermochim. Acta **188**, 333 (1991).
12. Criado J.M., Málek J., Ortega A.: Thermochim. Acta, **147**, 377 (1989).
13. Málek J., Criado J.M.: Thermochim. Acta **164**, 199 (1990).
14. Kissinger H.E.: Anal. Chem. **29**, 1702 (1957).
15. Ozawa T.: J. Therm. Anal. **2**, 301 (1979).
16. Ozawa T.: Bull. Chem. Soc. Jpn. **38**, 1881 (1965).
17. Friedman H.L.: J. Polym. Sci. Part C, **6**, 183 (1964).
18. Ozawa T.: J. Therm. Anal. **31**, 547 (1986).
19. Ozawa T.: Netsu Sokutei **1**, 2 (1974) (in Japanese).
20. Koga N., Málek J., Šesták J., Tanaka H.: Netsu Sokutei **20**, 210 (1993).
21. Málek J.: Thermochim. Acta **200**, 257 (1992).
22. Senum G.I., Yang R.T.: J. Therm. Anal. **11**, 445 (1977).
23. Málek J.: Thermochim. Acta **267**, 61 (1995).
24. Prime R.B. in *Thermal Characterization of Polymeric Materials*, (E.A. Turi Ed.), Chapt. 5, p. 435, Academic Press, New York 1981.
25. Barton J.M. in *Epoxy Resins and Composites I, Advances in Polymer Science* (K. Dušek Ed.), Vol. 72, p. 112, Springer Verlag, Berlin 1985.
26. Prime R.B.: Polym. Eng. Sci. **13**, 365 (1973).
27. Prowder T., Holsworth R.M., Grentzer T.H., Kline S.A. in *Polymer Characterization* (C.D. Craver Ed.), Adv. Chem. Series, Vol. 203, Chapt. 13, p. 233, Am. Chem. Soc., Washington 1983.
28. Montserrat S., Málek J.: Thermochim. Acta **228**, 47 (1993).
29. Montserat S.: J. Appl. Polym. Sci. **44**, 545 (1992).
30. Fava R.A.: Polymer **9**, 137 (1968).
31. Zukas W.X.: Polym. Eng. Sci. **29**, 1553 (1989).
32. Oleynik E.F. in *Epoxy Resins and Composites IV* (K. Dušek Ed.), Advances in Polymer Science **80**, p. 49, Springer-Verlag, Berlin 1986.
33. Havlíček I., Dušek K. in *Crosslinked Epoxies* (B. Sedláček and J. Kahovec Eds), p. 417, Walter de Gruyter, Berlin 1987.
34. Wisanrakkit G., Gillham J.: J. Coating. Technol. **62**, 35 (1990).
35. Marotta A., Buri A., Branda F., Saiello S. in *Nucleation and Crydstallization in Glasses*, (J.H. Simmons, D.R. Uhlmann and G.H. Beall Eds), Advances in Ceramics, Vol. 4, p. 146, Amer. Ceram. Soc., Ohio 1982.
36. Yinnon H., Uhlmann D.R.: J. Non-Cryst. Solids **54**, 273 (1983).
37. Matusita K., Sakka S.: Phys. Chem. Glasses **20**, 81 (1979).

38. Matusita K., Sakka S.: Phys. Chem. Glasses **20**, 81 (1979).
39. Suriñach S., Baró M.D., Clavaguera-Mora M.T., Clavaguera N.: J. Non-Cryst. Solids **58**, 209 (1983).
40. Henderson D.W., Ast D.G.: J. Non-Cryst. Solids **64**, 43 (1984).
41. Henderson D.W.: J. Non-Cryst. Solids **30**, 301 (1979).
42. Ryšavá N., Tichý L., Barta Č., Tříska A., Tichá H.: Phys. Status Solidi A, **87**, K13 (1985).
42. Ryšavá N., Spasov T., Tichý L.: J. Therm. Anal. **32**, 1015 (1987).
43. Ryšavá N., Barta Č., Tichý L.: J. Mat. Sci. Lett. **8**, 91 (1989).
44. Málek J., Černošková E.: J. Non-Cryst. Solids, to be published.
45. Volmer M., Weber A.: Z. Phys. Chem. **119**, 227 (1926).
46. Johnson W.A., Mehl R.F.: Trans. Am. Inst. Min. (Metall.) Engs. **135**, 416 (1939).
47. Avrami M.: J. Phys. Chem. **7**, 1103 (1939); **8**, 212 (1940); **9**, 177 (1941).
48. Kolmogorov A.N.: Izvestia Akad. Nauk USSR, Ser. Math. **1**, 355 (1937).
49. Christian J.W.: *The theory of Transformations in Metals and Alloys*, 2nd ed., Pergamon, New York 1975.
50. DeBruijn T.J.W., DeJong W.A., Van der Berg P.J.: Thermochim. Acta **45**, 315 (1981).
51. Shepilov M.P., Baik D.S.: J. Non-Cryst. Solids **171**, 141 (1994).
52. Subbarao E.C. in *Advances in Ceramics* (A.H. Heuer and L.W. Hobbs Eds), Vol. 3, Science and Technol. of Zirconia, p. 1, The Americam Ceramic Soc.1981.
53. Denkewicz R.P. Jr., TenHusein K.S., Adair J.H.: J. Mater. Res. **5**, 2698 (1990).
54. Blesa M.A., Maroto A.J.G., Passaggio S.I., Figliolia N.E., Rigotti G.: J. Mat. Sci. **20**, 4601 (1985).
55. Torralvo M.J., Alario M.A., Soria J.: J. Catal. **86**, 473 (1984).
56. Gimblett G., Rahman A.A., Sing K.S.W.: J. Chem. Tech. Biotech. 30, 51 (1980).
57. Ramanathan S., Soni N.C., Prasad R.: J. Mat. Sci. Lett. **12**, 122 (1993).
58. Arone A., Pernice P., Marotta A.: J. Mat. Sci. Lett. **10**, 1136 (1991).
59. Isobe T., Senna M.: J. Solid State Chem. **93**, 368 (1991).
60. Murase Y., Kato E.: J. Am. Ceam. Soc. **66**, 196 (1983).
61. Málek J., Mitsuhashi T., Ramírez J., Matsui Y.: J. Mat. Research, to be published.